The Influence of Coal Gangue Particle Gradation on the Performance of Inorganic Foamed Paste Backfill Materials

Chonghui Fu, Chunwei Wang, Fengshun Zhang, Hucheng Chai, Liya Zhao, Xuemao Guan, Jianping Zhu, Haibo Zhang*

Henan Key Laboratory of Materials on Deep-Earth Engineering, School of Materials Science and Engineering, Henan Polytechnic University, Jiaozuo 454003, China

*Corresponding author: Haibo Zhang, zzhb@hpu.edu.cn

Abstract: The issue of top contact in paste backfill materials is a common technical challenge in coal mine filling processes, and overcoming this problem has become a significant research direction in current studies and engineering practices. This paper utilizes coal gangue as aggregate and hydrogen peroxide as a foaming agent to prepare foamed paste backfill materials. Three close-packing theories were employed to investigate the effects of different coal gangue particle gradations on the mechanical properties, expansion ratio, water absorption, and dry density of foamed paste backfill materials under the same foaming agent content. The hydration mechanism and pore structure evolution were analyzed using XRD, SEM, and OSM techniques. The results indicate that when the hydrogen peroxide addition is 5%, the foamed paste backfill material regulated by MAA gradation theory exhibits the best comprehensive performance, achieving a 28-day compressive strength of 0.89 MPa, an expansion ratio of 155.5%, and a dry density of 1.24 g/cm^3. The regulation of coal gangue aggregate particle gradation not only improves the foaming efficiency but also allows the formation of CH to fill the material pores, enhancing the overall structural support capacity and forming a closer microstructure. This research provides new insights into controlling the properties of foamed paste backfill materials.

Keywords: Particle gradations; Coal gangue; Foamed paste backfill materials; Cement; Coal ash

1. Introduction

Coal is a crucial energy source for humanity, with high demand and intensive extraction processes [1, 2]. However, coal mining generates significant waste and underground voids, leading to issues such as land subsidence and groundwater pollution [3–8]. Currently, paste backfill technology is one of the effective technologies widely applied in recent years to manage underground voids, as illustrated in **Figure 1** [9]. Compared to traditional filling materials, paste backfill materials offer excellent flowability and high compressive strength, making them adaptable to various geological conditions and engineering environments [10]. Paste backfill materials is composed

of cementitious materials, supplementary cementitious materials (such as fly ash and slag), aggregates (such as coal gangue and slag), additives (such as retarders and water reducers), and water, mixed uniformly [11–17]. After mixing on the surface, paste backfill materials are typically transported by gravity or pumping. The hydrated paste backfill materials not only provide support to the surrounding rock but also ensure a safe working environment for miners.
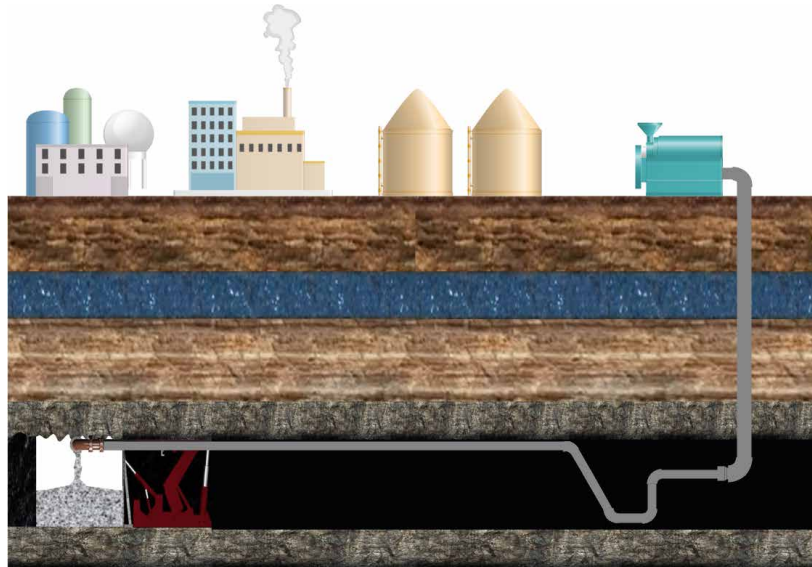

Figure 1. Paste backfill process

However, paste backfill materials typically require good fluidity during the pumping process, which results in a high water-to-binder ratio. This often leads to water loss and bleeding during placement and hydration. Additionally, the high proportion of aggregate in paste backfill materials can cause aggregate settlement, creating voids between the paste backfill material and the roof, preventing a compact contact with the roof and making it difficult to completely fill the goaf, thereby reducing the stability of the underground filling area, as shown in **Figure 2** [18, 19]. To date, several techniques have been proposed to overcome this issue, such as artificial roof-contacted, forced roof-contacted, and multi-point discharging [20]. These techniques can significantly improve the poor contact between paste backfill materials and the roof, but their high costs make them difficult to implement. Therefore, finding a cost-effective solution to the problem of poor roof contact has become a key research direction for paste backfill materials.

Figure 2. Gaps occurring in paste backfill roof contact

Foamed concrete is characterized by its advantages of volume expansion and minimal shrinkage, while its porous structure helps reduce local stress concentration, effectively addressing the aforementioned issues. Inspired by foamed concrete, incorporating foaming agents into paste backfill materials to create foamed paste backfill materials is an effective approach. Due to the high porosity of foamed paste backfill materials, they have lower density and poorer mechanical properties compared to traditional paste backfill materials. To enhance performance, current research on foamed paste backfill materials primarily focuses on mineral additives, dosage, and types and amounts of foam [21–25]. However, for coal gangue-based foamed paste backfill materials, cost constraints typically result in coal gangue aggregates comprising over 70% of the material. The content and gradation of these aggregates are decisive factors affecting the compaction performance and compressive strength of coal gangue-based foamed paste backfill materials [26].

This study systematically evaluates the impact of different coal gangue particle gradations on foamed paste backfill materials based on three-particle packing theories (Talbot gradation theory, MAA gradation theory, and the I method). The mechanical properties of the foamed paste backfill materials were assessed using a pressure testing machine, and the pore structure, microstructure, and phase composition were investigated using SEM, XRD, TG-DTG, and MIP techniques. The foaming mechanism and top contact process issues were theoretically analyzed, providing theoretical guidance for improving the stability and safety of goaf areas. **Figure 3** illustrates the effects achieved by the foaming top contact process.
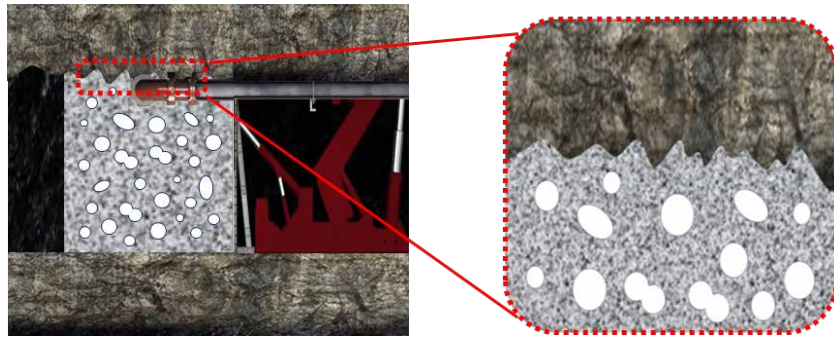

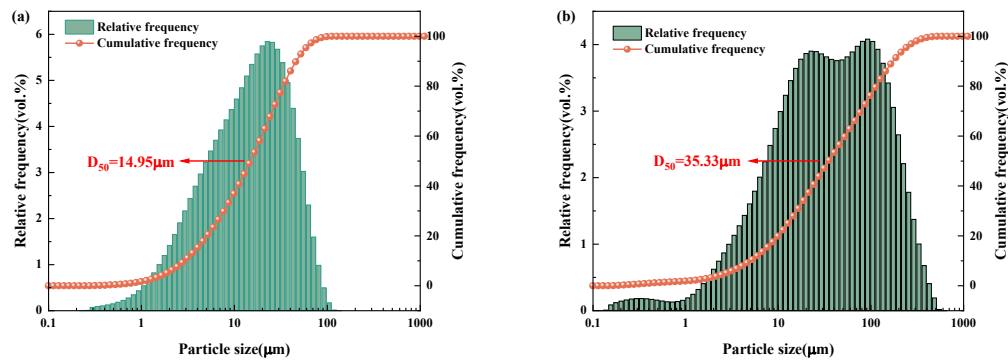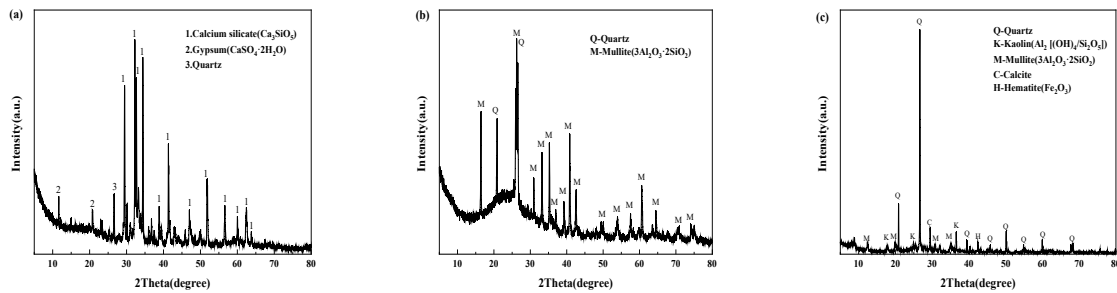**Figure 3.** Foam-based roof contact process

2. Experimental procedure

2.1. Raw materials

This study utilizes various raw materials to formulate foamed paste backfill materials. The primary raw materials include P·O 42.5 ordinary Portland cement (sourced from Jiaozuo Qianye Cement Co., Ltd.), industrial-grade fly ash, and coal gangue (both sourced from Shanxi Lu'an Environmental Energy Development Co., Ltd.). The admixture used is a water-reducing agent produced by Shanxi Sangmus Building Materials and Chemical Co., Ltd., and the foaming agent is hydrogen peroxide produced by Yantai Shuangshuang Chemical Co., Ltd. (with a density of 1.11 g/cm^3 and a concentration of 30%). The XRF analysis of the raw materials is presented in **Table 1**. The particle size distribution of the raw materials is shown in **Figure 4** and the XRD results are depicted in **Figure 5**.

Table 1. Chemical composition of raw materials(%)

Chemical composition	Cement	Fly ash	Coal gangue
SiO_2	21.95	49.33	57.59
Al_2O_3	7.99	30.15	21.31
Fe_2O_3	2.81	6.09	6.51
CaO	58.03	4.78	6.42
K_2O	0.88	1.15	3.51
TiO_2	0.41	1.08	1.24
Na_2O	0.57	0.73	1.03
MgO	3.44	0.70	0.99
SO_3	3.54	1.22	0.73
LOI	3.92	6.6	11.4

Figure 4. Particle size distribution of raw materials: (a) Cement; (b) Fly ash.

Figure 5. XRD result of raw materials(a) Cement;(b) Fly Ash;(c) Coal gangue.

2.2. Sample preparation

2.2.1. Preparation of foamed paste backfill material

The preparation process of paste backfill materials is illustrated in **Figure 6**. According to the proportions listed in **Table 2**, accurately weigh the raw materials (the amount of each particle size of coal gangue is calculated based on different close packing theories, with results shown in **Table 3**, **Table 4**, and **Table 5**). Sequentially add coal gangue, fly ash, and cement into the mixer, and dry mix them thoroughly. Gradually add water and a water-reducing agent over a period of 90 seconds. After all the water has been added, continue mixing for an additional 120 seconds. Then, pour hydrogen peroxide into the mixing bowl and stir for 6–8 seconds. Pour the mixture into

molds with dimensions of 100 mm × 100 mm × 100 mm for shaping. The molded samples are then placed in a standard curing room (20°C, 95% humidity) for curing.
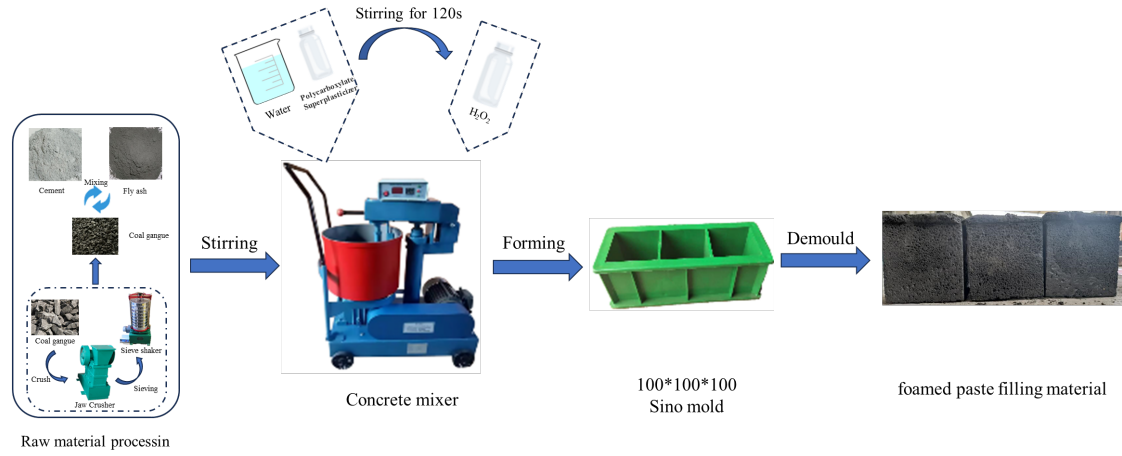

Figure 6. Detail steps for the preparation of paste backfill materials

Table 2. Paste backfill material proportion design(kg/m^3).

Cement	Fly ash	Coal gangue	Water reducer	Water	H$_2$O$_2$
180	270	1320	1.26	312	22.5

Based on the investigation of Fuller, a minimal porosity can be theoretically achieved by an optimal particle size distribution (PSD) of all the applied particle materials in the mix [27, 28]. Talbot also proposed a fitting equation based on the trend of the curve, as shown in Equation 1 below:

$$Y = 100 \left(\frac{D_0}{D_{max}} \right)^n \tag{1}$$

In this equation, $P(D)$ is a fraction of the total solids being smaller than size D, D is the particle size (μm), D_{max} is the maximum particle size (μm) and q is the distribution modulus.

Table 3. Percentage of cumulative sieve residue for Talbot theory

Label	n	Mass content (%) of particles passing through the following sieve pores (mm)							
		16	9.5	4.75	2.36	1.18	0.6	0.3	0.15
1	0.38	100.00	82.03	63.03	48.32	37.13	28.72	22.07	16.96
2	0.42	100.00	80.34	60.05	44.76	33.45	25.18	18.82	14.07
3	0.44	100.00	79.50	58.60	43.08	31.76	23.58	17.38	12.81
4	0.46	100.00	78.68	57.20	41.46	30.14	22.08	16.05	11.67
5	0.5	100.00	77.06	54.49	38.41	27.16	19.36	13.69	9.68

Dinger and Funk., through experimentation, suggested that in reality, there must be a finite lower size limit. Hence, they proposed a modified model based on the Andreasen and Andersen Equation, as shown in Equation 2 [29].

$$CPFT(\%) = 100 \left(\frac{D^q - D_S^q}{D_L^q - D_S^q} \right) \tag{2}$$

In this equation, CPFT(%) represents the cumulative percentage finer than a given particle size D; D_L denotes the maximum particle size in the system; D_S represents the minimum particle size in the system; D is the known particle size; q is the distribution coefficient.

Table 4. Percentage of cumulative sieve residue for MAA grading theory

Label	q	Mass content (%) of particles passing through the following sieve pores (mm)							
		16	9.5	4.75	2.36	1.18	0.6	0.3	0.15
1	0.17	100.00	85.84	68.86	53.64	40.24	28.60	17.98	8.54
2	0.21	100.00	84.68	66.73	51.09	37.69	26.38	16.33	7.64
3	0.25	100.00	83.47	64.58	48.56	35.22	24.25	14.78	6.82
4	0.29	100.00	82.23	62.41	46.06	32.82	22.23	13.33	6.06
5	0.33	100.00	80.97	60.24	43.61	30.52	20.33	11.99	5.36

Based on the study of the maximum packing density curve theory, particle interference theory, and related grading algorithms, a calculation formula was proposed using the percentage passing decrement rate i as a parameter, known as the I method, as shown in Equation 3 [30]:

$$P_i = 100(i)^{(x)} \qquad\qquad (3)$$

In this equation, Pi represents the percentage passing through the x-th sieve size (%); i is the decrement rate of the particle passing percentage, ranging from 0.7 to 0.8; the series , where dx is the corresponding square sieve opening size for each particle grade (e.g., 16, 13.2, 9.5, ..., 0.075 mm).

Table 5. Percentage of cumulative sieve residue for i-method theory

Label	i	Mass content (%) of particles passing through the following sieve pores (mm)							
		16	9.5	4.75	2.36	1.18	0.6	0.3	0.15
1	0.7	100.00	76.48	53.55	37.37	26.16	18.48	12.94	9.06
3	0.72	100.00	78.12	56.26	40.39	29.09	21.11	15.21	10.95
5	0.74	100.00	79.75	59.02	43.56	32.24	24.04	17.79	13.17
7	0.76	100.00	81.36	61.84	46.89	35.64	27.27	20.73	15.76

2.2.2. Preparation of test samples

The preparation of samples is illustrated in **Figure 7**. The preparation process of test samples is as follows: The paste backfill blocks are precisely cut into different sizes for various microstructural analyses. For XRD testing, one-sixteenth of the block is taken, crushed, and hydration is terminated using alcohol. The sample is then dried at a constant temperature of 50°C until a stable mass is achieved. The dried sample is ground to pass through a 200-mesh standard sieve. MIP test samples are prepared as regular rectangular prisms with dimensions of 10mm ± 1mm in length and width and a height not exceeding 20mm ± 1mm. All samples are soaked in anhydrous ethanol for 48 hours to terminate hydration reactions, followed by drying at 50°C.
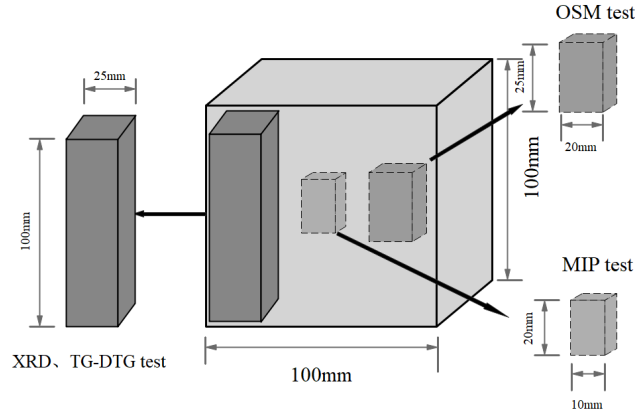
Figure 7. Schematic diagram of microscopic sample preparation.

2.3. Test methods

2.3.1. Bulk density and expansion ratio

Using a plastic measuring cup, weigh the mass M of 1000 ml of paste with the foaming agent, and record the volume V after foaming ceases. The weight of the plastic measuring cup is m. The bulk density is calculated as shown in Equation 4. The expansion ratio is the ratio of the final volume to the initial volume of 1000 ml.

$$\gamma = \frac{M-m}{V} \tag{4}$$

2.3.2. Dry density

Three test blocks are taken, and the length, width, and height of each block are measured in three directions. The average of six measurements is used as the length value in each direction. The volume V of each test block is calculated. The three blocks are placed in a drying oven at a temperature of (60 ± 5) °C until the mass difference between two consecutive measurements, 4 hours apart, is no more than 1g. After removal, the dry mass m0 of the test block is weighed, accurate to 1g. The dry density is calculated as shown in Equation 5. The dry density is the average of the three blocks, accurate to 1 kg/m³.

$$\rho_0 = \frac{m_0}{V} \tag{5}$$

2.3.3. Water absorption

The immersion process for determining dry density uses a graded immersion method. The test block is placed in a constant temperature water environment at (20 ± 5) °C, proceeding in three stages: first, immersed to 1/3 of the block height for 24 hours, then water is added to 2/3 height for another 24 hours, and finally, water is added to exceed the block surface by 30mm for a further 24 hours. After immersion, the block is removed, surface free water is wiped off with a damp cloth, and the mass mg is immediately weighed (accuracy 1g). The water absorption rate W is calculated as shown in Equation 6. The water absorption rate should be the average of the three test blocks, accurate to 0.1%.

$$W = \frac{m_g - m_0}{m_0} \times 100\% \tag{6}$$

2.3.4. Compressive strength

The samples continue standard curing to the predetermined age (3, 7, 28 days) to test the compressive strength of the paste cubes. A universal testing machine is used to test the mechanical properties of the samples, with a loading

rate of 0.5mm/s during testing. The test results are determined by the average of three samples.

2.3.5. Mercury intrusion porosimetry (MIP)

The mercury intrusion porosimetry (MIP) method is used to measure the cumulative porosity and pore size distribution of the samples. MIP characterizes pores larger than 3nm, with a pressure range of 0.1–30000 psia, using a full scan mode and a contact angle of 130°.

2.3.6. Scanning electron microscope (SEM)

After curing to the specified age, the test blocks are crushed, and the flaky paste material is soaked in anhydrous ethanol to terminate hydration for 48 hours, then dried in a 50°C oven. A scanning electron microscope (SEM) from Carl Zeiss NTS GmbH, Merlin Compact, is used for SEM testing. Before testing, the samples are vacuumed and gold-sputtered. Secondary electron testing is conducted at 10kV.

2.3.7. X-ray Diffraction(XRD)

X-ray diffraction (XRD) is used to analyze phase changes in samples as the proportion of coal gangue powder increases. Prepared powder samples are analyzed using a high-resolution powdered X-ray diffractometer (XRD, Cu target). The test voltage is 45 KV, the current is 150 mA, the scan step is 0.02°, the scan speed is 5°/min, and the test range is 5–80°.

2.3.8. Thermogravimetric analysis(TGA)

Thermogravimetric analysis (TGA) is used to analyze the decomposition process of samples at high temperatures. Approximately 20mg of sample powder is weighed, and thermal analysis is conducted using an STA8122/H comprehensive thermal analyzer. The test is conducted under a nitrogen atmosphere, with a heating rate of 10°C/min, a temperature range of 25–1000°C, and a gas flow rate of 20 mL/min.

2.3.9. Optical super depth-of-field microscope (OSM)

The pore structure of the foamed paste backfill material is observed using a Leica DVM6 ultra-depth-of-field microscope from Leica Microsystems. The treated samples are placed on a microscope carrier with a magnification of 30× for observation.

3. Results

3.1. Water absorption, expansion ratio, dry density, and compressive strength

Figure 8 illustrates the effects of different coefficients in three close packing theories on the water absorption, expansion ratio, dry density, and compressive strength of foamed paste backfill materials.
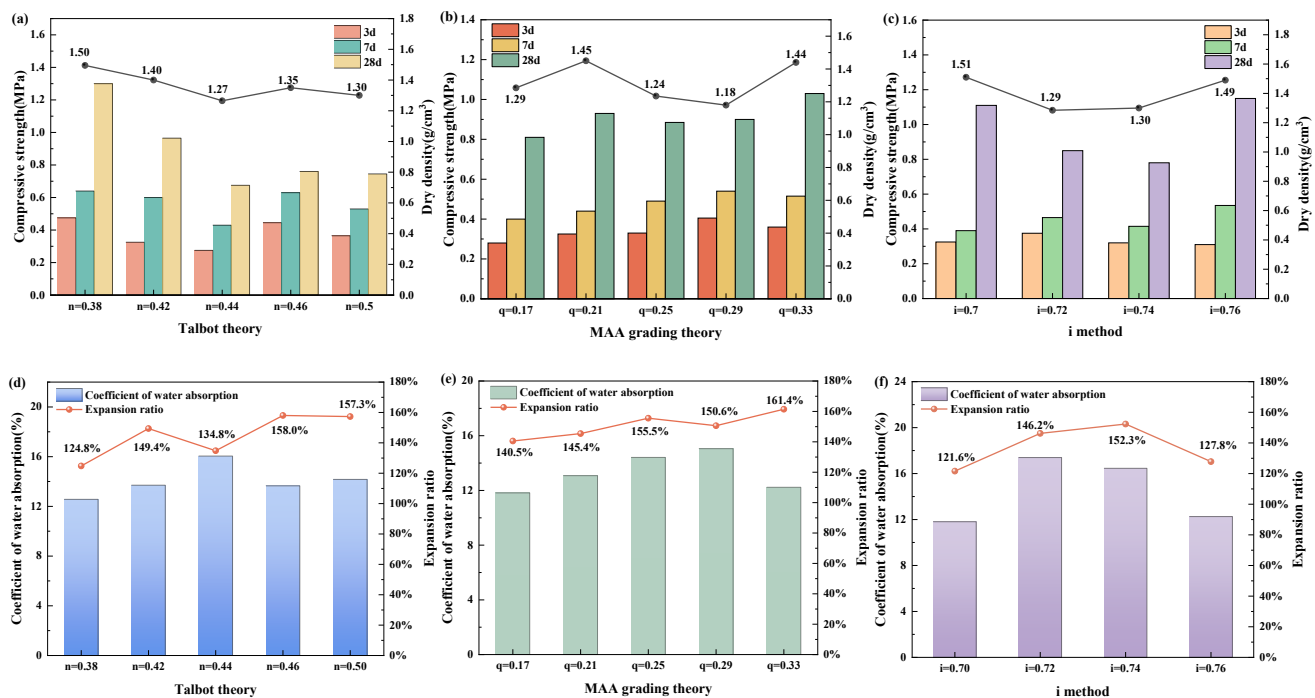
Figure 8. The influence of different close packing theories on macroscopic properties: (a–c) the influence of Talbot theory, MAA grading theory, and i method on compressive strength and dry density; (d–f) the effects of Talbot theory, MAA grading theory, and i method on water absorption and expansion ratio.

Figure 8 (a) and **(d)** show that in the Talbot theory, as the coefficient n increases, the dry density and compressive strength initially decrease and then increase, while the water absorption first increases and then decreases, and the expansion ratio exhibits a stepwise increase. This is because, in the Talbot theory, with an increase in n, the proportion of coarse coal gangue (16mm–4.75mm) increases, while the proportion of fine coal gangue (4.75mm–0.15mm) decreases. The overall specific surface area of the coal gangue decreases with increasing n, allowing the same amount of hydrogen peroxide to achieve a greater expansion ratio. The change in aggregate particle gradation provides more reaction interfaces for hydrogen peroxide, facilitating bubble diffusion and expansion in the paste. When n = 0.44, the expansion ratio decreases while water absorption increases, due to the agglomeration of coal gangue observed during foaming. The generation of bubbles causes partial aggregation of coarse coal gangue, increasing the number of open pores and thus reducing compressive strength. At n = 0.46 and n = 0.50, both the expansion ratio and dry density increase because these groups have a higher proportion of coarse coal gangue compared to the previous groups, resulting in a heavier overall material.

Figure 8 (b) and **(e)** indicate that in the MAA gradation theory, as the coefficient q increases, the dry density and compressive strength first increase, then decrease, and increase again, while the water absorption first increases and then decreases. The expansion ratio shows a trend of first increasing, then decreasing, and increasing again. In the MAA gradation theory, both compressive strength and expansion ratio are relatively better compared to the other two close packing theories. As shown in **Table 4**, the lower content of coal gangue powder results in a relatively higher free water content in the paste, making bubble generation easier. However, higher fluidity is not always beneficial. In the MAA gradation theory, the proportion of coal gangue powder (0.15mm–0.074mm) is less than in the other two theories. As q increases, the proportion of coal gangue powder decreases, making it difficult for the paste to encapsulate the coal gangue, reducing the cohesiveness of the foamed paste backfill material,

leading to aggregate settlement and segregation. After adding the foaming agent, newly formed bubbles cause the aggregate to float. Due to the relatively high density of the aggregate, those initially at the top layer gradually move downward, but bubbles may burst during the movement of coal gangue, explaining why the expansion ratio increases while the dry density rises at q=0.33.

Figure 8 (c) and (f) demonstrate that in the i method theory, the macroscopic performance trends are similar to those in the Talbot theory. As the coefficient i increases, the proportion of coarse coal gangue decreases, while the proportion of fine coal gangue increases, leading to an initial rise and subsequent fall in the expansion ratio. This phenomenon occurs because a higher proportion of coal gangue powder results in less free water in the paste, reducing the foaming effect. The results indicate that in foamed paste backfill materials, the paste must have a certain cohesiveness to effectively encapsulate bubbles, preventing their escape and avoiding aggregate settlement [31]. Good particle gradation can also enhance compressive strength [32]. On the other hand, an excessive proportion of coal gangue powder can lead to poor paste fluidity, making bubble generation difficult and failing to achieve effective top contact [33].

3.2. MIP

Figure 9 illustrates the impact of different coefficients of three close-packing theories on the porosity of foamed paste backfill materials.
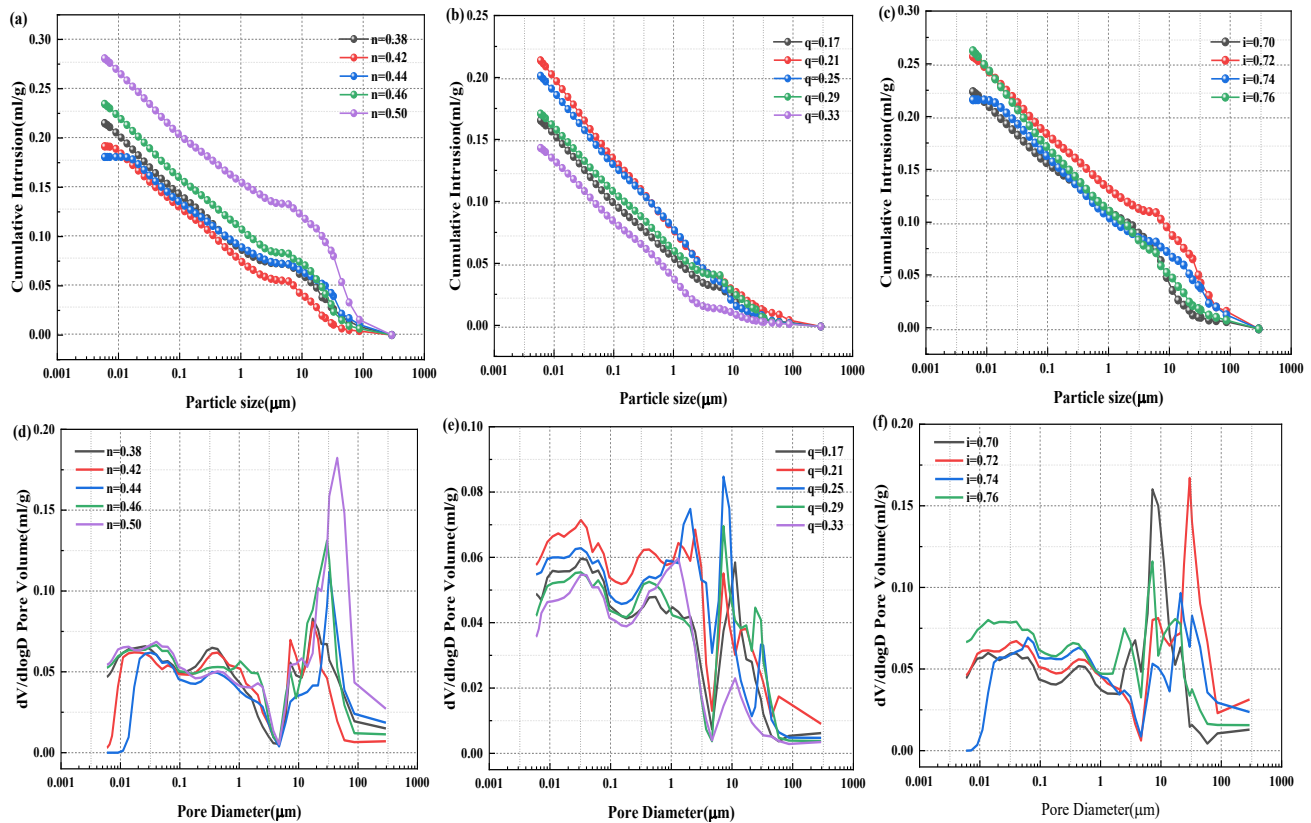

Figure 9. MIP curves of sample with different close packing theories: (a–c) cumulative pore distribution of Talbot theory, MAA grading theory and i method theory, respectively. (d–f) dV/dlogD pore volume of Talbot theory, MAA grading theory and i method theory, respectively.

It can be observed from the figure that changes in the gradation of coal gangue aggregate particles significantly affect pores larger than 10μm within the cementitious system. In Figure 9(a) and (d), the overall porosity change according to the Talbot theory is not significant. However, as the coefficient n increases from 0.38 to 0.50, there is a trend where pores larger than 10μm first decrease and then increase. This is because, at

n = 0.38, the higher proportion of coal gangue powder results in less free water within the paste, reducing its fluidity and thus the foaming efficiency of the foaming agent. Additionally, due to the closer cementitious system, bubbles generated by the foaming agent cannot diffuse into the surrounding area, and the high viscosity of the paste prevents bubble coalescence, leading to most pores being smaller than 10μm. As the coefficient n increases, the proportion of coarse coal gangue rises while that of fine coal gangue decreases, reducing the overall specific surface area of the coal gangue. This increases the free water content in the paste, allowing bubbles generated by the foaming agent to diffuse more easily. Furthermore, the decreased viscosity of the paste increases the likelihood of bubble coalescence, resulting in more bubbles larger than 10μm. At n = 0.5, the paste's viscosity is insufficient to stabilize the bubbles, leading to a collapse.   In **Figure 9(b)** and **(e)**, the overall pore distribution according to the MAA gradation theory is more uniform compared to the other two theories, with the overall porosity first increasing and then decreasing. This phenomenon is mainly attributed to the uniform distribution of aggregate particle sizes in the MAA gradation theory, along with a relatively low content of coal gangue powder, which prevents excessive paste viscosity and uneven foaming, thereby enhancing overall strength and bubble stability.

In **Figure 9(c)** and **(f)**, the pore size distribution according to the i method is similar to that of the Talbot theory, with a larger proportion of pores over 10μm. This can lead to decreased bubble stability and increased water absorption of the foamed paste backfill material, which may result in material failure under conditions such as coal mine goafs. For foamed paste backfill materials, a good pore size distribution can reduce stress concentration and improve the overall strength and durability of the material [34, 35].

3.3. Sectional view

Figure 10, Figure 11, and **Figure 12** illustrate the effects of different coefficients in three close-packing theories on the aggregate distribution in foamed paste backfill materials. Based on the analysis, the coefficients selected for the study were n = 0.42, 0.44, 0.46 in the Talbot theory, q = 0.17, 0.21, 0.25, 0.29 in the MAA gradation theory, and i=0.72, 0.74, 0.76 in the i method.

From **Figure 10**, it can be observed that under the Talbot theory, as the coefficient changes, the overall aggregate distribution is more uniform when n = 0.46. This is because as n increases, the viscosity of the paste decreases. On one hand, this facilitates the generation and diffusion of bubbles within the paste, forming a uniform bubble structure, but it can also lead to bubble coalescence, resulting in larger bubbles. On the other hand, coal gangue aggregates are more evenly dispersed in the paste, significantly enhancing the fluidity of the paste and reducing aggregate agglomeration.
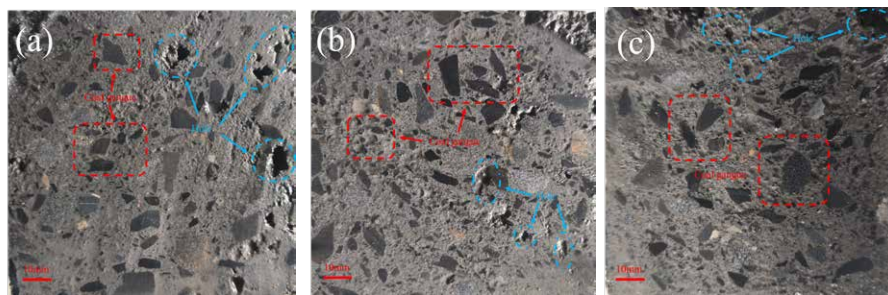

Figure 10. Cross-sectional images of samples with Talbot theory: (a) n = 0.42; (b) n = 0.44; (c) n = 0.46.

Figure 11 shows that under the MAA gradation theory, when q = 0.25, the aggregate distribution within the cross-section exhibits a high degree of uniformity. In the MAA gradation theory, the content of coal gangue powder is relatively low, and as the coefficient increases, the viscosity of the paste gradually decreases. This not only causes aggregates to potentially settle under gravity, leading to stratification, but also causes bubbles to

rise and burst rapidly. When q = 0.29, it is evident that aggregates concentrate in certain areas, which can lead to uneven physical and mechanical properties, affecting the performance of the foamed paste backfill material.
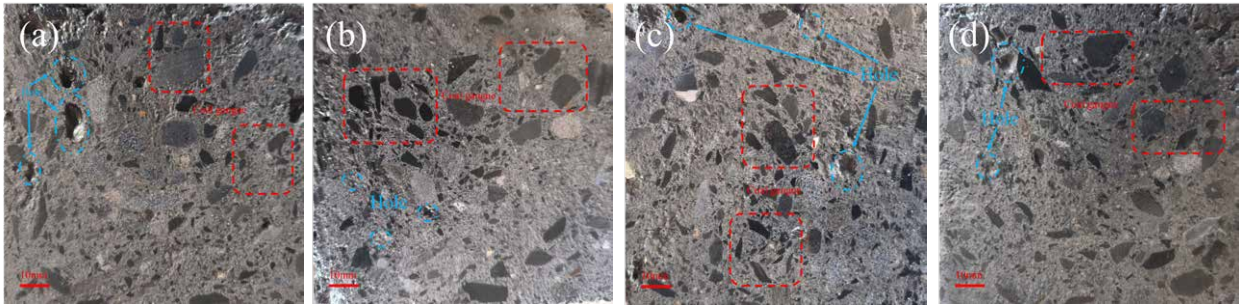

Figure 11. Cross-sectional images of samples with MAA grading theory: (a) q = 0.17; (b) q = 0.21; (c) q = 0.25; (d) q = 0.29.

From **Figure 12**, it is evident that in the I method, when i = 0.74, the aggregate distribution is more uniform compared to the other two groups. This phenomenon occurs because, as the coefficient i changes, the content of coarse coal gangue in the paste gradually decreases while the content of fine coal gangue increases, leading to increased paste viscosity. An appropriate paste viscosity can prevent aggregates from settling or floating, ensuring their uniform distribution.
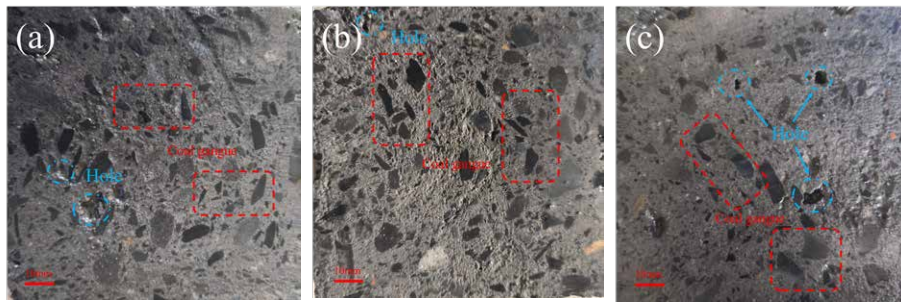

Figure 12. Cross-sectional images of samples with i method theory: (a) i = 0.72; (b) i = 0.74; (c) i = 0.76.

The above results indicate that in foamed paste backfill materials, uniformly distributed aggregates can effectively support the foamed structure, while also helping to reduce material deformation and aggregate settlement, thereby enhancing structural stability.

3.4. OSM

The impact of three close-packing theories on the pore structure of foamed paste backfill materials is illustrated in **Figure 13**. Based on the aforementioned analysis, three sample groups with superior comprehensive performance were selected from the three close-packing theories. Due to the rough surface of the samples and the tendency for some coal gangue aggregates to be mistaken for bubbles, Image Pro Plus was used to process the images and calculate the average pore size, as shown in **Table 6**.

Figure 13 reveals that bubbles smaller than 1mm constitute a significant proportion and numerous irregular bubbles appear in the coal gangue foamed paste materials. This phenomenon arises because, during the foaming process, the high density of coal gangue causes it to move within the paste, while external forces acting on the bubbles lead to uneven foaming and deformation. The average pore size also indicates that when q = 0.25, the average pore size is relatively the smallest, which helps form a more uniform and stable foam structure, enhancing the overall strength and stability of the material and reducing the risk of material fracture. This is partly due to changes in aggregate particle gradation, which alter the viscosity of the paste, affecting bubble formation and

stability. Higher viscosity aids bubble stability but may inhibit bubble formation. Lower viscosity allows bubbles to form and spread more easily within the paste but can lead to thinner bubble walls, increasing the risk of bubble rupture. It also affects the paste's flowability, thereby influencing bubble formation and distribution.

Additionally, changes in aggregate particle gradation affect the material's compactness; coarse aggregates can form an aggregate structure, while fine aggregates fill the voids between coarse aggregates, creating a more stable matrix structure that supports bubble stability. Furthermore, aggregate particle gradation may influence the distribution and effectiveness of the foaming agent within the paste, thereby affecting the foaming outcome. Therefore, by reasonably adjusting particle gradation, the foaming effect can be optimized, enhancing the material's performance and quality [36].

Table 6. Average pore size of samples with different close packing theories.

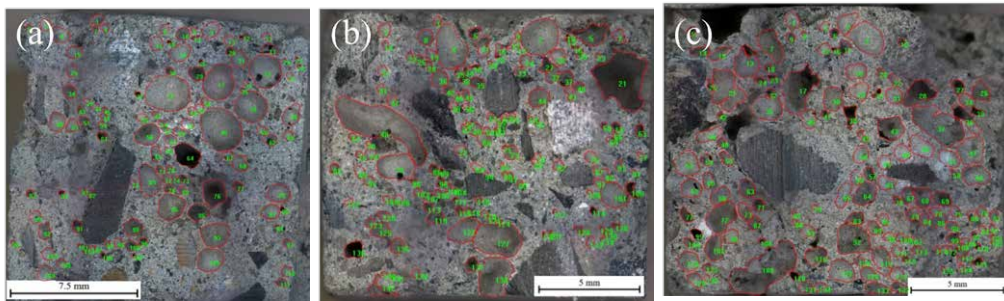| Sample	n = 0.46	q = 0.25	i = 0.74
Average pore size/μm	744.9	504.3	672.0

Figure 13. Pore structure of samples with different close packing theories: (a) n = 0.46; (b) q = 0.25; (c) i = 0.74.

3.5. SEM

Figure 14 illustrates the impact of three close packing theories on the microstructure of 28-day foamed paste backfill materials. It can be observed that variations in particle gradation significantly affect the distribution of hydration products. In **Figure 14(a)**, most of the cement hydration products are encapsulated on the surface of coal gangue, with a considerable amount of unreacted fly ash particles present internally. The internal microstructure in **Figure 14(c)** is quite similar to that in **Figure 14(a)**. In **Figure 14(b)**, the C-S-H gel produced by cement hydration connects the surrounding coal gangue and fly ash particles, forming a closer structure. A uniform particle gradation distribution facilitates the formation of close C-S-H gel, thereby enhancing the material's strength.
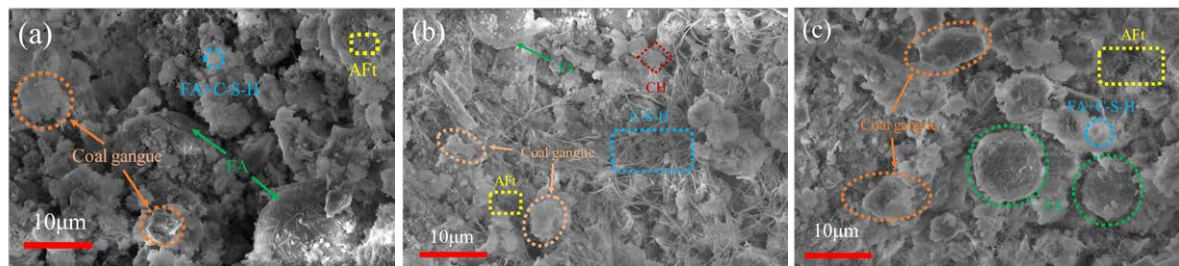

Figure 14. SEM image of samples with different close packing theories: (a) n = 0.46; (b) q = 0.25; (c) i = 0.74.

3.6. XRD

Figure 15 shows the effect of three close packing theories on the hydration products of 28-day foamed paste backfill materials.
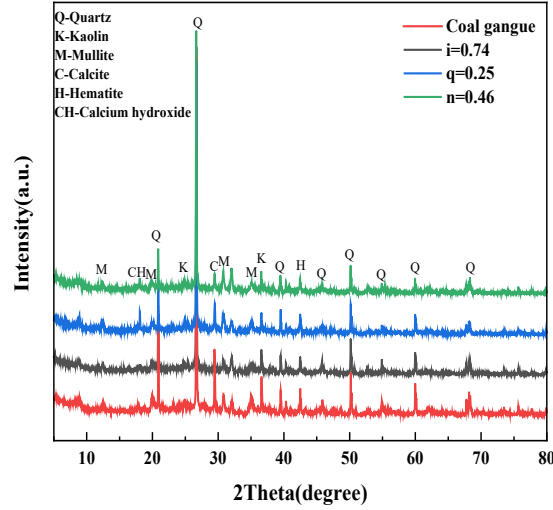
Figure 15. XRD of samples with different close packing theories.

It is evident that changes in particle gradation have a significant impact on the phase composition. After adding cement and fly ash to the specimens, diffraction peaks of minerals such as quartz and mica are still present, but their heights have decreased, indicating a reduction in the relative content of quartz and mica, leading to a decrease in their XRD peak intensity. Additionally, different particle gradations result in corresponding changes in the calcium hydroxide content within the specimens. This is because variations in particle gradation affect the foaming efficiency of hydrogen peroxide.

Firstly, the particle gradation of coal gangue influences the pore structure of the mixture. A better gradation may provide a more uniform pore distribution, thereby affecting the decomposition of hydrogen peroxide and bubble formation. Secondly, particle gradation may affect the contact area between hydrogen peroxide and the cement paste, influencing its decomposition rate and foaming efficiency. Finally, the foaming efficiency of hydrogen peroxide impacts the hydration reaction of cement (e.g., by altering the pore structure or moisture distribution), and the increase in water released from hydrogen peroxide decomposition increases the solubility of calcium hydroxide, affecting its content in the specimens.

3.7. TG-DTG

Figure 16 presents the TG-DTG curves of paste materials based on three close packing theories.
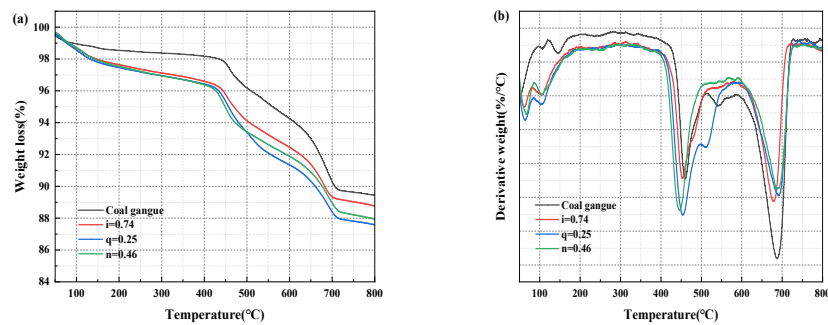

Figure 16. TG and DTG curves of samples with different close packing theories: (a) mass loss curves; (b) derivative of mass loss curves.

Each group of specimens exhibits a small absorption peak between 60–200°C, accompanied by a certain amount of mass loss, corresponding to the loss of free water, adsorbed water, and weakly bound water in the gel [37, 38]. In the 200–400°C range, the mass loss mainly results from the continued dehydration of the gel [39]. Between 400–600°C, the dissociation of large molecular functional groups in coal gangue, hydroxyl removal, and calcium hydroxide decomposition occurs [40]. In the 600–800°C range, a significant endothermic peak is observed, indicating the presence of calcium carbonate [41].

By comparing the different close packing theories, variations in coal gangue particle gradation lead to shifts in the weight loss peaks at each stage. In the 60–200°C range, there are differences in the gel content. In the 400–600°C range, the decomposition of calcium hydroxide produced by cement hydration causes a shift in the weight loss peak, indicating differences in calcium hydroxide content, consistent with the XRD analysis results.

4. Discussion

4.1. Effect of aggregate particle size on foam backfill material

The intermolecular forces on the surface of liquid-phase substances create surface tension. When the surface tension is too high, molecules cannot overcome this force to form bubbles [42].

Upon adding a foaming agent to the cement paste, gases produced by chemical reactions accumulate within the paste, causing volume expansion. Eventually, the bubbles solidify to form a porous filling material.

The formation mechanism of foamed materials can be summarized as the evolution process of foam cells, as shown in **Figure 17**. This process mainly includes three stages:

(1) Nucleation: gas is introduced or generated by the decomposition of the foaming agent.
(2) Bubble growth: the initial gas nuclei gradually expand.
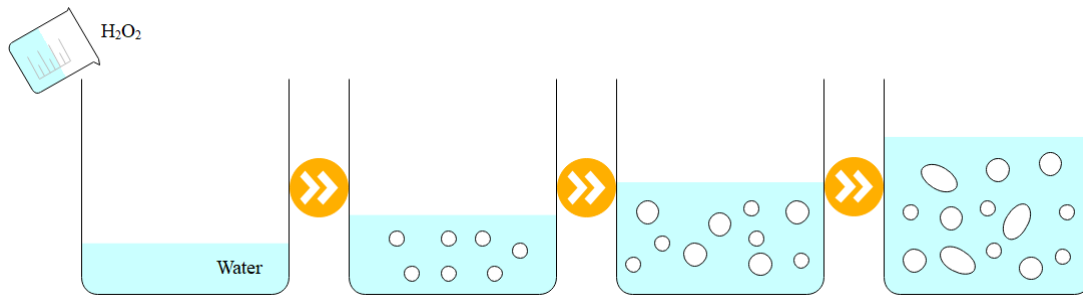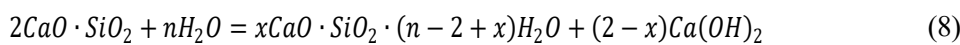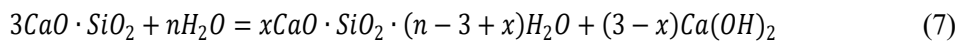(3) Structure stabilization: the configuration of bubbles stabilizes during the hardening of the cement paste.

Figure 17. Hydrogen peroxide foaming process

Due to the presence of peroxide bonds and low symmetry, hydrogen peroxide easily undergoes decomposition reactions. When hydrogen peroxide is added to the cement paste, the alkaline environment within the paste accelerates its decomposition. The reactions of cement are shown in Equation 7 and Equation 8.

$$3CaO \cdot SiO_2 + nH_2O = xCaO \cdot SiO_2 \cdot (n-3+x)H_2O + (3-x)Ca(OH)_2 \qquad (7)$$

$$2CaO \cdot SiO_2 + nH_2O = xCaO \cdot SiO_2 \cdot (n-2+x)H_2O + (2-x)Ca(OH)_2 \qquad (8)$$

From these chemical reaction equations, it can be seen that the cement paste becomes alkaline due to the calcium hydroxide produced by the reaction between cement and water. At this point, the reaction of hydrogen peroxide is shown in Equation 9, Equation 10, and Equation 11.

$$2H_2O_2 \rightarrow 2H_2O + O_2 \uparrow \qquad (9)$$

$$H_2O_2 \Leftrightarrow H^+ + HOO^- \qquad (10)$$

$$H_2O_2 + HOO^- \rightarrow H_2O + OH^- + O_2 \uparrow \qquad (11)$$

As shown in Equation 10, the reaction is reversible, and a stronger alkaline environment in the cement paste increases the hydroxide ion concentration, driving the reaction to the right, thereby increasing the concentration of [HOO]$^-$. According to Equation 11, the increased [HOO]$^-$ accelerates the decomposition of hydrogen peroxide, creating the necessary conditions for foaming in the paste.However, in the process of accelerating the reaction rate of hydrogen peroxide, it is not sufficient to merely pursue faster reactions, as bubbles are thermodynamically unstable systems [43]. The bubbles produced cannot be preserved permanently and may collapse.

The formation and stability of bubbles are mainly influenced by two factors: Firstly, the surface tension of the liquid plays a decisive role in bubble formation. Excessive surface tension hinders the process of water molecules detaching from the liquid surface to encapsulate gas. Increasing the viscosity of the solution can effectively reduce surface tension, creating conditions for the stable existence of bubbles.

Secondly, the gravitational drainage effect of the liquid film significantly affects bubble stability. Due to the density difference between liquid and gas, the liquid moves downward under gravity, causing the upper part of the liquid film to thin and eventually rupture. Additionally, the presence of large particles in the system can move downward due to gravity, accelerating the bubble rupture process. Therefore, controlling the viscosity of the paste and optimizing particle stability are key to maintaining the bubble structure.

Figure 18 illustrates the foaming behavior when hydrogen peroxide is added to coal gangue paste. Under identical conditions, the proportion of coarse to fine coal gangue plays a crucial role in the foaming effect. A high proportion of coarse coal gangue can lead to a decrease in paste viscosity and an increase in surface tension, directly affecting the stability and distribution of bubbles. Although the presence of coarse coal gangue can promote bubble generation, the reduced viscosity of the paste prevents bubbles from being fully encapsulated, causing them to easily escape from the paste. This hinders the bubbles from performing their intended function, affecting foam generation and stability.

Due to the higher density of coal gangue, its gravitational effect causes it to settle at the bottom of the paste. During this settling process, coal gangue may collide with bubbles, leading to bubble rupture, which further reduces the foaming ratio. The instability and collapse of bubbles can result in a loose paste structure, decreasing overall strength and stability. This not only affects production efficiency but may also lead to subsequent process issues. Conversely, an excessively high proportion of fine coal gangue may overly increase the paste's viscosity, affecting its flowability and causing uneven foaming. A balanced proportion of coarse and fine coal gangue can enhance the strength of the foamed paste, help form a stable bubble structure, and prevent bubble rupture or uneven distribution.
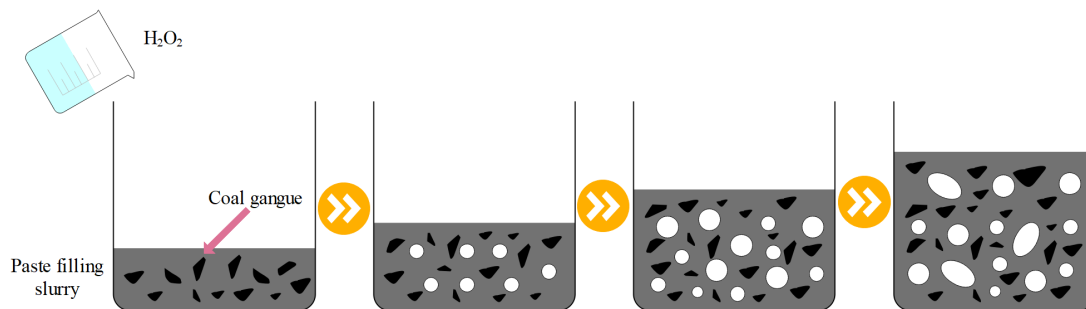

Figure 18. The foaming process of hydrogen peroxide in paste backfill paste.

4.2. Engineering application

Currently, the issue of top contact in paste backfill presents a common technical challenge in coal mine filling processes, primarily involving the contact and support effectiveness between the filling system and the roof. Insufficient fluidity of the paste, uneven roof surfaces, and paste settlement are key reasons for the failure of paste backfill to achieve top contact. **Figure 19** illustrates the phenomenon of paste backfill failing to achieve top contact. The inability of paste backfill to achieve top contact impacts mine safety in several ways:

(1) The filling system cannot closely contact the roof, leading to inadequate support and increasing the risk of roof collapse or caving incidents.

(2) The filling system that fails to achieve top contact cannot effectively bear and distribute ground pressure, resulting in pressure concentration in localized areas.

(3) The filling system that fails to achieve top contact cannot fully perform its supporting function, leading to wastage of filling materials.

Figure 19. Diagram of paste backfill material failing to reach the roof

Figure 20 shows the condition of paste backfill materials achieving top contact after the addition of a foaming agent. To enhance the overall strength of paste backfill, a portion of non-foamed paste is first injected, followed by the addition of a foaming agent at the pipeline outlet. The mixing device at the pipeline outlet mixes the foaming agent with the paste, and the mixed foamed paste is then injected into the area requiring top contact. The spontaneous action of the foaming agent allows the paste material to achieve close top contact, thereby enhancing structural stability and safety. This method reduces costs, effectively fills irregular voids, ensures close contact with the roof, enhances the overall load-bearing capacity of the structure, and reduces the risk of roof collapse.
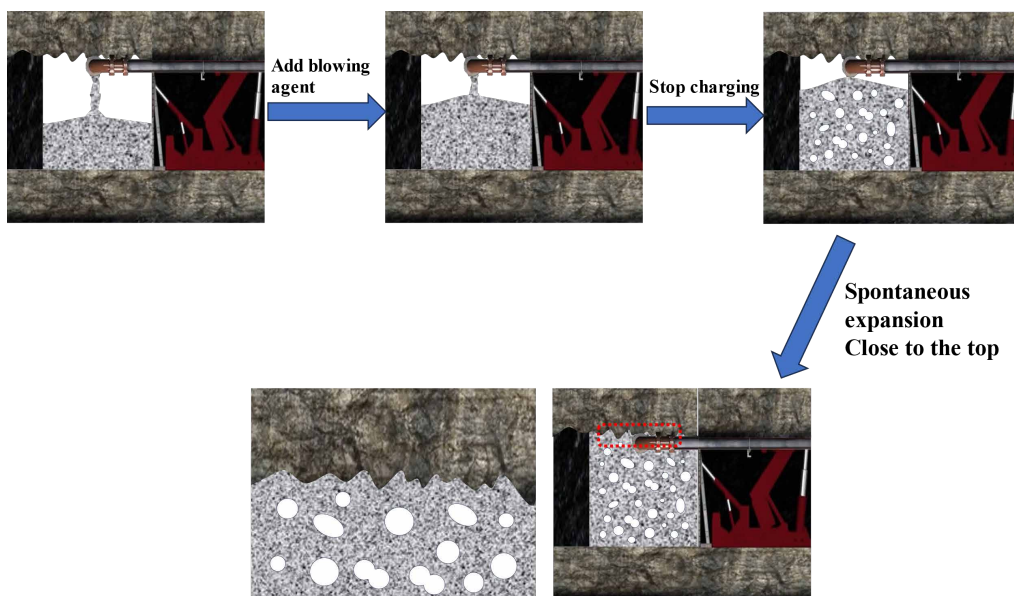

Figure 20. Foaming roof contact process

5. Conclusion

The above study demonstrates that employing different close packing theories to regulate the gradation of coal gangue aggregates significantly impacts the performance of foamed paste backfill materials. Based on the mechanical properties and microstructure of these materials, the main conclusions are as follows:

(1) In the Talbot theory, the performance of foamed paste backfill with coal gangue is optimal when the coefficient n = 0.46. The 28-day compressive strength is 0.76 MPa, the expansion ratio is 158.0%, and the dry density is 1.35 g/cm³.

(2) In the MAA gradation theory, the performance is optimal when the coefficient q = 0.25. The 28-day compressive strength is 0.885 MPa, the expansion ratio is 155.5%, and the dry density is 1.24 g/cm³.

(3) In the i method theory, the performance is optimal when the coefficient i = 0.74. The 28-day compressive strength is 0.78 MPa, the expansion ratio is 152.3%, and the dry density is 1.3 g/cm³.

(4) When considering only the particle gradation of coal gangue aggregates, the results derived from the three close packing theories differ. Comparing the optimal results of these theories reveals that the foamed paste backfill material regulated by the MAA gradation theory exhibits a more uniform distribution of aggregates and pores within the material, with a relatively smaller average pore size.

(5) The impact of different particle gradations on performance varies. It not only affects the foaming efficiency of the foaming agent but also influences the hydration reaction. Specifically, particle gradation affects the internal CH content, which contributes to enhancing the overall structural support capacity of the material. An appropriate amount of CH helps fill the voids, improving the volumetric stability of the material

(6) Currently, the issue of top contact in paste backfill presents a common technical challenge in coal mine filling processes. The development of foamed paste backfill materials not only addresses the problem of inadequate contact with the roof but also enhances the overall load-bearing capacity of the structure, thereby reducing the risk of roof collapse and lowering costs.

Funding

Disclosure statement

The authors declare no conflict of interest.

References

[1] Song G, Du K, Zhang Y, et al., 2023, Study of the Overlying Strata Movement Law for Paste-Filling Longwall Fully Mechanized in Gaohe Coal Mine. Applied Sciences, 13(14): 8017.

[2] Du Z, Chen D, Li X, et al., 2024, Study on the Partial Paste Backfill Mining Method in a Fully Mechanized Top-Coal Caving Face: Case Study from a Coal Mine, China. Sustainability, 16(11): 4393.

[3] Hu Y, Hu R, Zhang B, et al., 2024, Research on Mechanical Properties and Mix Proportion Design of Solid Waste-Based Cemented Paste Backfill. Case Studies in Construction Materials, 21: e03618.

[4] Wang H, Chen D, Guo R, et al., 2023, A Preliminary Study on the Improvement of Gangue/Tailing Cemented Fill by Bentonite: Flow Properties, Mechanical Properties and Permeability. Materials, 16(20): 6802.

[5] Li L, Huang Q, Zuo X, et al., 2022, Study on the Slurry Diffusion Law of Fluidized Filling Gangue in the Caving Goaf

of Thick Coal Seam Fully Mechanized Caving Mining. Energies, 15(21): 8164.

[6] Wu P, Zhao J, Jin J, 2023, Similar Simulation of Overburden Movement Characteristics under Paste Filling Mining Conditions. Scientific Reports, 13(1): 12550.

[7] Hou C, Zhu W, Yan B, et al., 2018, Influence of Binder Content on Temperature and Internal Strain Evolution of Early Age Cemented Tailings Backfill. Construction and Building Materials, 189: 585–593.

[8] Yang L, Yilmaz E, Li J, et al., 2018, Effect of Superplasticizer Type and Dosage on Fluidity and Strength Behavior of Cemented Tailings Backfill with Different Solid Contents. Construction and Building Materials, 187: 290–298.

[9] Wang Y, Fall M, Wu A, 2016, Initial Temperature-Dependence of Strength Development and Self-Desiccation in Cemented Paste Backfill that Contains Sodium Silicate. Cement and Concrete Composites, 67: 101–110.

[10] Emad MZ, Mitri H, Kelly C, 2018, Dynamic Model Validation Using Blast Vibration Monitoring in Mine Backfill. International Journal of Rock Mechanics and Mining Sciences, 107: 48–54.

[11] Yin S, Yan Z, Chen X, et al., 2022, Effect of Fly-Ash as Fine Aggregate on the Workability and Mechanical Properties of Cemented Paste Backfill. Case Studies in Construction Materials, 16: e01039.

[12] Wang B, Yang L, Li Q, et al., 2024, Mechanical Behavior, Acoustic Emission and Principal Strain Field Evolution Properties of Layered Cemented Paste Backfill under Unconfined Compression. Construction and Building Materials, 415: 135111.

[13] Xu B, Li Y, Li J, et al., 2024, Nonlinear Stress Growth and Failure Characteristics of Gangue-Cemented Backfill. Construction and Building Materials, 424: 135938.

[14] Wang Z, Wu A, Wang S, et al., 2024, Effect and Mechanism of Time-Dependent and Economical Expansion Materials in Improving the Active Roof-Contact for Cemented Paste Backfill. Construction and Building Materials, 439: 137339.

[15] Li Q, Wang B, Wei Z, et al., 2024, Experiment and Numerical Simulation Study of Polycarboxylate Superplasticizer Modified Cemented Ultrafine Tailings Filling Slurry: Rheology, Fluidity, and Flow Properties in Pipeline. Construction and Building Materials, 438: 137041.

[16] Yunpeng K, Guangbo L, Zepu S, et al., 2024, Experimental Study on the Evolutive Shear Fracture Behaviour and Properties of Cemented Paste Backfill. Construction and Building Materials, 423: 135780.

[17] Zhang C, Wang J, Song W, et al., 2024, Study on Shear Behavior and Microstructure of Rock and Cemented Paste Backfill Interface. Construction and Building Materials, 443: 137834.

[18] Hefni M, Hassani F, 2020, Experimental Development of a Novel Mine Backfill Material: Foam Mine Fill. Minerals, 10(6): 564.

[19] Li MY, Guo LJ, Zhao Y, et al., 2024, A State-of-the-Art Review on Delayed Expansion of Cemented Paste Backfill Materials. Rare Metals, 43(8): 3475–3500.

[20] Kouame KJA, Feng Y, Jiang F, et al., 2015, A Study of Technical Measures for Increasing the Roof-Contacted Ratio in Stope and Cavity Filling. Journal of Materials Science Research, 5(1): 54–60.

[21] Ercikdi B, Cihangir F, Kesimal A, et al., 2010, Utilization of Water-Reducing Admixtures in Cemented Paste Backfill of Sulphide-Rich Mill Tailings. Journal of Hazardous Materials, 179(1): 940–946.

[22] Koohestani B, Belem T, Koubaa A, et al., 2016, Experimental Investigation into the Compressive Strength Development of Cemented Paste Backfill Containing Nano-Silica. Cement and Concrete Composites, 72: 180–189.

[23] Fall M, Pokharel M, 2010, Coupled Effects of Sulphate and Temperature on the Strength Development of Cemented Tailings Backfills: Portland Cement-Paste Backfill. Cement and Concrete Composites, 32(10): 819–828.

[24] Ngo I, Ma LQ, Zhao ZY, et al., 2024, Sol–Gel-Stabilized CO_2 Foam for Enhanced In-Situ Carbonation in Foamed Fly Ash Backfill Materials. Geomechanics and Geophysics for Geo-Energy and Geo-Resources, 10(1): 80.

[25] Xu XCA, Sun XG, Yao W, et al., 2021, Strength and Ultrasonic Characteristics of Cemented Paste Backfill Incorporating Foaming Agent. MINERALS, 11(7): 681.

[26] Li H, Wang H, Bai L, 2024, Effect of Coal Gangue Grading Characteristics on Cemented Paste Backfill Rheology. Case Studies in Construction Materials, 21: e03694.

[27] Fuller WB, Thompson SEJ, 1907, THE LAWS OF PROPORTIONING CONCRETE. 59: 67–143.

[28] Xiang JC, Liu LP, Cui XM, et al., 2019, Effect of Fuller-Fine Sand on Rheological, Drying Shrinkage, and Microstructural Properties of Metakaolin-Based Geopolymer Grouting Materials. Cement and Concrete Composites, 104: 103381.

[29] Yu R, Spiesz P, Brouwers HJH, 2014, Mix Design and Properties Assessment of Ultra-High Performance Fibre Reinforced Concrete (UHPFRC). Cement and Concrete Research, 56: 29–39.

[30] Peng B, 2005, Gradation Design Method Based on Method of i Change. Journal of Wuhan University of Technology(Transportation Science and Engineering), 29(5) 751–754.

[31] Xiang G, Song D, Li H, et al., 2023, Investigation on Preparation and Compressive Strength Model of Steel Slag Foam Concrete. Journal of Building Engineering, 72: 106548.

[32] Han S, Zhang P, Zhang H, et al., 2023, Physical and Mechanical Properties of Foamed Concrete with Recycled Concrete Aggregates. Frontiers in Materials, 10: 01–14.

[33] Ni K, Shi Y, Hu Z, et al., 2020, Effect of Coal Gangue Grain Size on Strength of Foam Concrete. Journal of Physics: Conference Series, 1635(1): 012080.

[34] Wei H, Liu Y, Wu T, et al., 2020, Effect of Aggregate Size on Strength Characteristics of High Strength Lightweight Concrete. Materials, 13(6): 1314.

[35] Chung SY, Abd Elrahman M, Kim JS, et al., 2019, Comparison of Lightweight Aggregate and Foamed Concrete with the Same Density Level Using Image-Based Characterizations. Construction and Building Materials, 211: 988–999.

[36] Abd Elrahman M, El Madawy ME, Chung SY, et al., 2019, Preparation and Characterization of Ultra-Lightweight Foamed Concrete Incorporating Lightweight Aggregates. Applied Sciences, 9(7): 1447.

[37] Deboucha W, Leklou N, Khelidj A, et al., 2017, Hydration Development of Mineral Additives Blended Cement Using Thermogravimetric Analysis (TGA): Methodology of Calculating the Degree of Hydration. Construction and Building Materials, 146: 687–701.

[38] Fordham CJ, Smalley IJ, 1985, A Simple Thermogravimetric Study of Hydrated Cement. Cement and Concrete Research, 15(1): 141–144.

[39] Carriço A, Real S, Bogas JA, et al., 2020, Mortars with Thermo Activated Recycled Cement: Fresh and Mechanical Characterisation. Construction and Building Materials, 256: 119502.

[40] Romano RCdO, Bernardo HM, Maciel MH, et al., 2019, Using Isothermal Calorimetry, X-ray Diffraction, Thermogravimetry and FTIR to Monitor the Hydration Reaction of Portland Cements Associated with Red Mud as a Supplementary Material. Journal of Thermal Analysis and Calorimetry, 137(6): 1877–1890.

[41] Jin J, Li M, Liu T, et al., 2024, Insights into Factors Influencing Coal Gangue-Filled Backfill Cemented by Self-Consolidating Alkali-Activated Slag Grouts. Construction and Building Materials, 411: 134422.

[42] Hu N, Liu Y, Ke L, et al., 2023, Preparation and Frothing Mechanism of Froth Concrete Based on Solid Waste: A Review. Construction and Building Materials, 401: 132831.

[43] Hou L, Li J, Lu Z, et al., 2021, Influence of Foaming Agent on Cement and Foam Concrete. Construction and Building Materials, 280: 122399.